Title

Subtitle

Max Sharnoff
Trinity 2022
candidate number
BA Computer Science

Abstract

Detecting changes in human lung morphology and determining its effects on lung function requires significant time committment per patient, so statistical analysis on many individuals is infeasible. Computational models of the lung are therefore a natural choice for researching the effects of altered lung morphology, with reference to existing lung function tests.

Accurate computational models also allow investigation into properties of the lungs that cannot feasibly be measured; e.g., increased internal stress in one location from damaged airways elsewhere.

This paper builds on recent advancements in modelling airflow in the lungs (⟨reference to Foy⟩) to produce an efficient, accurate model of the lungs that supports simple alterations to the simulated morphology. We then use this model to determine the strains placed on the rest of the lungs by various kinds of constricted or damaged airways.

Contents

1 Introduction

1.1 Motivation

Respiratory diseases account for more than 10% of *all* disability-adjusted life-years lost due to any medical condition, second only to cardiovascular diseases.[1] Because of this, any betterment of our understanding of the lungs and how they change from damage has immediate benefits towards understanding one of the most significant categories of disease.

In spite of this, there are relatively few existing methods for experimentation. Clinical observations on live patients are necessarily limited, and common techniques – spirometry, inert-gas washout, and fMRI imaging – all have severe limitations that render them infeasible or impossible to use for obtaining detailed data on the lungs at scale. And on top of that, the difficulty of drawing inference from these methods is enhanced by the fact that they are purely observational; in this paper, we are concerned with the effects of certain changes in lung morphology (such as: tightening of the airways, stiffness in the expansion and contraction, etc.).

Of course, it would be unethical to *induce* these changes in patients. However, sufficiently-accurate computational models present a natural solution. By designing models that can easily be arbitrarily deformed or otherwise altered, we create the opportunity to efficiently investigate how targeted changes in lung morphology affect both lung functioning as a whole and the stresses placed on individual regions.

Todo: **I'd like to add something along the lines of: "historically, computational models have been too expensive for experimentation without specialized equipment, but recent developments (i.e. Foy) have show other methods for simulating airflow are both efficient and accurate."**

1.2 Contributions to the field

This paper introduces a new tool for simulating and observing changes to the lungs, and their precise effects.

Todo: **Something about: "this is useful to people looking to find new results about *how* the lungs get impacted by various diseases." Would like to also say: "we have investigated the effects of clinically-observed symptoms from a couple diseases, to showcase the utility of this tool"**

2 Background

2.1 Physiology of the lungs

At a high level, the physiology of the lungs can be divided into the few most significant structures. This section does not discuss pulmonary blood circulation, or the mechanics of gas exchange – this paper is primarily concerned with the flow of air in and out of the lungs.

The flow of air into the lungs begins with the diaphragm, a muscle below the lungs that contracts to increase the volume of the *thoracic cavity* (where lungs are housed). This increase in volume causes the negative pressure that drives inspiration. Correspondingly, typical expiration is driven by relaxation of the diaphragm and the associated increase in pressure in the thoracic cavity.

Air flows into the body through the nose and mouth, meeting the trachea at the larynx, in the neck. The trachea splits into the left and right bronchi – connecting to the left and right lungs respectively. The bronchi split into a binary tree of progressively smaller bronchial tubes (the *tracheobronchial tree*), with the *generation* of a bronchial tube referring to the number of branches between it and the larynx. The smallest bronchial tubes terminate in a small number of acini, small clusters of alveoli. Alveoli are the small, spherical air sacs that act as the sites of gas exchange with the blood. A core technique used in this paper is the approximation of one or many acini as spherical air sacs themselves, further described in subsection 3.1. Typical dimensions for all of the structures above are given in Table 1.

Beyond the structure of the lungs, there are also a number of measures of volume. *Tidal volume* (TV) refers to the volume of air moved in or out of the lungs during a typical breath, and *functional residual capacity* (FRC) refers to the total volume of air remaining in the lungs after a normal expiration.[1] Typical values for TV and FRC are also given in Table 1.

Metric	Mean value (adult female)	Mean value (adult male)
Trachea length	todo	todo
Trachea radius	todo	todo
Bronchus length	todo	todo
Bronchus radius	todo	todo
Acinus radius	todo	todo
Alveolus radius	todo	todo
TV	todo	todo
FRC	todo	todo

Table 1: Typical sizes of various lung structures and volumes. Larger structures and effects tend to be more different in proportion between average males and females.

[1] **N.B.:** TV and FRC both describe typical breaths; there are analogous terms for maximum capabilities (*vital capacity* (VC) and *residual volume* (RV)). Also notable is *total lung capacity* (TLC; equal to VC + RV). These are included here for context, but they are not necessary for understanding the experiments in this paper.

2.2 Clinical methods

There are a number of relevant clinical methods for measuring lung function, many of which will be discussed in this section. Despite the clinical utiltiy however, there are certain limitations to these methods that make them less well-suited to research, namely: difficulty with establishing causation and cost per datapoint (either monetary, temporal, or both).

Reservations aside, current clinical tools for measuring lung function can essentially be grouped into three categories: exhalation measurement: spirometry and inert-gas washout; oscillometry: FOT and IOS; or imaging techniques: CT, PET, and MRI.

Spirometry measures the volume and flow from a patient's maximal exhalation (after maximal inhilation), producing volume-flow and volume-time curves. It is simple to perform, but the reliance on maximal exhalation gives it a particularly low sensitivity. *Inert-gas washout* instead floods the lungs with an inert gas (e.g. SF_6 or ^3He) before continuously measuring the concentration of the gas exhaled through normal breathing. Measurements are either made over many breaths (*multiple-breath washout* (MBW)) or just one (*single-breath washout* (SBW)). Both MBW and SBW have a number of indices typically produced from the data, which correlate with many lung diseases.

Both *forced oscillation technique* (FOT) and *impulse oscillometry* (IOS) apply oscillations at the mouth and measure the resulting airflow and pressure. FOT uses controlled pulses whereas IOS uses pseudo-random noise. From this, estimates of resistance and inertance of the lungs are made, which have correlations to diseases such as asthma and COPD.

Finally, we have the imaging techniques: *Magnetic resonance imaging* (MRI), *computed tomography* (CT), and *positron emission tomography* (PET). Beyond immediately-visible ailments (e.g. foreign objects or fluid buildup), these methods can also be used to estimate the ventilation of air in each voxel of the image – providing metrics that can quantify overall lung function (and highlight specific regions where function is degraded). However, these methods are typically expenive (MRI) or dangerous in large amounts (CT and PET) and the timeline of resolution improvements means that high-resolution imaging has not been available for as long as other methods. The costs associated with these methods and the relative recency of high-resolution versions has meant that there is also a relative gap in the literature linking imaging results to respiratory disease classification.

This final point is one of the key reasons why computational models are so useful; high costs or low availability hinder new research, and computer simulation can provide a simpler, cheaper method for testing ideas. It is difficult to obtain large amounts of data for analysis when the underlying methods are expensive or time-consuming, relative to the amount of data produced.[2]

Also of note is that all of the above techniques are strictly observation with respect to the condition of the lungs. Analyzing the effects of various morphological changes within the lungs is difficult without the ability to directly effect those

[2]To be clear here: methods like spirometry are relatively cheap and not overly time-consuming, but the amount of data each test generates is small; establishing complex relationships may require large amounts of data, regardless of the type of test used.

changes, but forced changes to patient lung morphology are typically both risky and unethical.

For those reasons, it is natural to turn to simulations – in particular, computational models – in order to gain insight into impact on physiology and overall function from isolated changes within the lungs.

2.3 Prior computational models

This section is unfortunately brief – historically, computational models have been limited by the available resources (they still are) and data to base them on. From the beginning, simulating "full" fluid dynamics with the Navier-Stokes equations has been both unnecessary and out of reach; reasonable assumptions can be made about the flow of air within the lungs to simplify modelling (see: subsection 3.1), and models have increased in complexity over time to match advancements in the speed of computers.

Early models represented the lungs with just a few elastic chambers, but advancements in physiological data (particularly from Weibel, 1963) allowed later models to generate larger models of the lungs, with the size now singularly limited by computational capabilities.

More recently, models have been partially constructed with results from patient imaging (up to generations 6-10) with later generations generated by the parameters from Webiel (1963).

Todo: **the "Weibel, 1963" above needs to actually be a reference**

3 Methods

Broadly speaking, this section comes in two parts; first defining the more theoretical underpinnings of the model used for simulation throughout the rest of the paper, followed by some detail on the implementation in practice. Much of the theory is adapted from [2], with minor modifications.

At a high level, we approximate the structure of the lungs *acinar regions* and represent the effects of the diaphragm as *pleural pressure* outside these acinar regions. The simulation itself uses the implicit Euler method, giving strong numerical stability at the cost of solving a complex system of equations (Equation 4) at each timestep.

At the implementation level, we modify the naive equations above to improve floating-point accuracy, and demonstrate the benefits of using sparse matrices – even without particularly complex solver methods.

3.1 Approximating the lungs

As with any computer simulation of physical processes, approximation is required on some level, due to the inherent limitations of classical computers. There are three distinct simplifications made for the purposes of computational feasibility that we will discuss here.

The first of these simplifications is that we assume our airflow is one-dimensional and incompressible. Modelling air inside the lungs as three dimensional or compressible could be more accurate, but would also require significantly more computational resources. Indeed, the key result of [2] is that making this simplification for airflow in the lungs retains the accuracy of the model – the small-scale differences that may be different from complex airflow modelling do not appear to affect the large-scale behavior.

We also approximate the movement of the diaphragm and expansion and contraction of the thoracic cavity with a singular measure of *pleural pressure*, a uniform pressure exerted on all the acini in the lungs. Some prior work uses a gradient for pleural pressure, modelling the effects of gravity. We chose to omit this for simplicity, due to the relatively small magnitude of these gradients[3] As a consequence, the position of each bronchial tube in a given model does not affect the mechanics of its simulation.

Finally, we simulate groups of many acini at once by modelling them as a single, balloon-like air sac. The average human pair of lungs contains approximately 300 million acini – far too many to assign unique variables to each one in a system of equations. So we approximate arbitrarily large numbers of acini as *acinar regions*, modelling their elastic behavior and interaction with the pleural pressure in the same way as individual acini would be.

[3] [2] draws upon prior studies to use a gravitational gradient strength of 2%/cm, meaning that the maximum and minimum pleural pressures at a given point in time differ by exactly 2%.

Todo: **actually I'm not sure what's going on here. the units in the equation don't work. (page 29 [pdf pg 34])**

3.2 Simultaneous equations

This section provides a summary and brief description of the four simultaneous equations that govern the state of our system, the first of which is the following:

$$P_{\text{parent}(i)} - P_i = R(i)Q_i \tag{1}$$

This specifies that the pressure differential between the distal end of branch i and its parent must equal the pressure from the resistance from the flow through this branch i. For the "root" branch, $P_{\text{parent}(i)}$ is the pressure at the trachea – typically atmospheric pressure.

The resistance term $R(i)$ is defined as following function, as given by Pedley et al. (1970):

$$R(i) = \frac{2\mu L_i c}{\pi r_i^4} \left(\frac{4\rho |Q_i|}{\mu \pi L_i} \right)^{\frac{1}{2}}$$

The parenthesized term corresponds to the Reynold's number of the flow, scaled by the ratio of the diameter of the branch to its length L_i. r_i is the radius of branch i, μ is the viscosity of the air, and $c = 1.85$ is a correction constant.

The second equation ensures incompressibility; the flow through a bifurcation must equal the sum of the flow through its children:

$$Q_i = \sum Q_{\text{child}} \tag{2}$$

where each *child* refers to any branch c with $\text{parent}(c) = i$.

The third equation maintains that the volume of an acinar region changes with the flow into or out of it for the given timestep:

$$V_i^t = V_i^{t-1} + dtQ_i^t \tag{3}$$

where dt is the timestep size, t refers to the current timestep, and V_i is the volume of the acinar region of branch i.

The final equation defines the elastic force of each acinar region, relating the pressure it exerts on its branch to the volume of the region itself and the pressure outside it:

$$P_i = \frac{1}{C_i} V_i + P_{pl}(t) \tag{4}$$

where $P_{pl}(t)$ is the pleural pressure (i.e. the "pressure" from the diaphragm, outside the acinar region) at the current time and C_i is the *compliance* of the acinar region of branch i. The pleural pressure changes over time to mimic human breathing patterns – hence why it is parameterised by t.

3.3 Modelling in the abstract

We use an *implicit* Euler method to model the system as it progresses: at each timestep, our simulation updates its state to the value of an approximate solution to the system of equations above. Equation 4 provides the necessary bounds to

make the method implicit, giving us higher accuracy at the cost of implementation complexity.

To solve for an approximate solution at each timestep, we use Newton's method with $f_{\boldsymbol{S}}(\boldsymbol{x})$ as defined below, iterating until $\|f_{\boldsymbol{S}}(\boldsymbol{x})\|^2 \leq tol$ and $\|dx\|^2 \leq tol$, with a tolerance of 10^{-6}. The two "inputs" – $\boldsymbol{S}$ and $\boldsymbol{x}$ – partition the state of the model into the variables that are controlled externally (e.g.: pleural pressure, compliance) and those that are calculated from the system state (e.g.: acinar volume, airflow). The definitions of $\boldsymbol{x}$ and $f_{\boldsymbol{S}}$ are given by:

$$x = (P_i..., Q_i..., V_i...)$$

$$f_{\boldsymbol{S}}(\boldsymbol{x}) = \begin{bmatrix} P_{\text{parent}(i)} - P_i - R(i)Q_i \\ \vdots \\ Q_i - \sum Q_{\text{child}} \\ \vdots \\ V_i^t - V_i^{t-1} - dtQ_i^t \\ \vdots \\ P_i - P_{pl}(t) - \frac{1}{C_i}V_i \\ \vdots \end{bmatrix}$$

Note that the values in $\boldsymbol{x}$ and equations in f are repeated only as many times as fits; e.g., there are fewer acinar regions than total branches, so there are fewer components in $\boldsymbol{x}$ from each V_i than from each Q_i.

As $\boldsymbol{S}$ only exists in the abstract sense, we won't bother to define its structure; all that's necessary to know is that it contains every variable referred to in f that is not already given explicitly by $\boldsymbol{x}$.

It's worth noting that in practice, the above definitions are only *nearly* correct; a few adjustments were made to the inputs and equations to mitigate limitations from floating-point accuracy. These are discussed in the next section.

3.4 Modified equations for floating-point accuracy

During initial experimentation, it became apparent that – under certain conditions – the pressure differential between ends of the bronchial tubes became too small for floating-point calculations to represent the changes in pressure during updates from Newton's method. This was because the absolute magnitude of the pressure (around 1e6 Pascals) was significantly different from the differences in pressure (much less than 1 Pascal).[4] We mitigated this by changing the formulation of the equations used in the simulation, improving their accuracy without changing their semantic meaning.

[4]**N.B.:** The change in pressure from *timestep-to-timestep* was still large enough to represent, but the changes to dx during the Newton iteration were. While it initially resolved by the methods in this section, this problem would have also been far lesser with 64-bit floating-point values (which we did eventually switch to).

The "new" equations gain accuracy by centering values closer to a magnitude of 1, so that the required number of significant digits is greatly reduced.[5] These equations use two new values, $\hat{P}$ and $\hat{V}$, that are relative to atmospheric pressure. They are defined by:

$$\hat{P} = P - P_{\text{atm}} \tag{5}$$

where P_{atm} is is atmospheric pressure; and:

$$\hat{V} = V - V|_{P=P_{\text{atm}}} \tag{6}$$
$$= C(\hat{P} - P_{pl}) \tag{7}$$

Note that the definition of $\hat{V}$ would be the result of simply substituting $\hat{P}$ for P in Equation 4. Applying these substitutions gives the following equations, equivalent to their counterparts above:

$$\hat{P}_{\text{parent}} - \hat{P}_i = R(i)Q_i \tag{8}$$

$$Q_i = \sum Q_{\text{child}} \tag{9}$$

$$\hat{V}_i^t = \hat{V}_i^{t-1} + dtQ_i^t \tag{10}$$

$$\hat{P}_i = \frac{1}{C_i}\hat{V}_i + P_{pl}(t) \tag{11}$$

Representing the pressure and volume by their *offset* from values at atmospheric pressure causes them to cluster much closer to zero – the magnitude of the mean is significantly decreased, relative to the variance of the values. This of course greatly improves the accuracy of each Euler step.

The same substitutions also apply to our representations of the state of the model and the optimization function used for Newton's method, as shown in subsection 3.3.

3.5 Sparse matrices

A key observation that aiding in simulation speed is that the Jacobean of our optimization function f has only $\mathcal{O}(n)$ entries – which allows for dramatic storage space and runtime savings. This optimization is crucial for practically running simulations up to a high depth on a single computer.

Please also note: The approximate pressures described here might be, but are not necessarily, reflective of pressures in the final simulation; there were multiple issues fixed after this observation that may have impacted these values. Even still, the modification was kept, as it provided a non-zero benefit.

This problem was detected while simulating unrestricted models, where the relative ease of flow means that the pressure throughout the lungs remains much more balanced.

[5] Floating-point numbers have a fixed number of significant digits; arithmetic operations with large differences in magnitude tend to lose significant information in the process.

We used sparse matrices, solving the equations with a sparse gaussian elimination. Other methods (such as GMRES) were initially considered but not used, due in equal parts to lack of library support and the sufficiency of the simpler gaussian elimination.[6] The increase in execution speed from dense to sparse matrices is quite significant, as demonstrated in Figure 1. The observed time for a simulation tick – which is roughly proportional to the time spent solving the system of equations – is still not linear in the number of nodes, however: fitting the sparse matrix timings to a power series model gives an exponent of 1.97 and R^2 of 0.989. Fitting a power series to the dense matrix timings gives an exponent of 3.35 and R^2 of 0.997; clearly significantly worse.

Todo: **not familiar with statistical language. what's the best way to write the sentences above?**

Although the improvement from $\mathcal{O}(x^{3.35})$ to $\mathcal{O}(x^{1.97})$ is significant, it is possible that other orderings of values within the Jacobean may be better-optimized for sparse gaussian elimination. Figure 2 provides a visual comparison between the sparsity pattern that was used in the software developed for this paper and a hypothetical alternative. The current layout used places all variables and equations of a certain type at consecuitve indexes, i.e. $(P\ldots, Q\ldots, V\ldots)$ instead of e.g. $(P_0, Q_0, V_0,\ P_1, Q_1, V_1,\ \ldots)$, with variables and equations for parent nodes occuring at *later* indexes.

As context for Figure 2 however, it is important to note that it is not possible for the system of equations to be simply organized into an upper- or lower-triangular matrix; each equation is composed of at least two variables. With this option unavailable, we did not assess alternate orderings of values within the Jacobean.

3.6 Procedural lung generation & configuration

As part of the simluation software developed for this paper, there are a number of configurable parameters – primarily encapsulating the structure of the lungs and how they change over the course of the simulation. Listing them exhaustively, the parameters are:

- Lung structure (the tree formed by the relationship between branches)
- Branch length, as relative to the parent
- Branch radius (healthy & degraded), relative to the parent
- Acinar region *relative compliance* (healthy & degraded)
- Branch angles (only affects the lungs' appearance)
- Keyframe-based scheduling to shift the lung state between healthy & degraded
  - Multiple interpolation functions to transition between keyframes

[6] There are, of course, *many* sparse matrix libraries in existence. The project was written in Rust, which – at time of writing – did not have more advanced sparse matrix solvers.

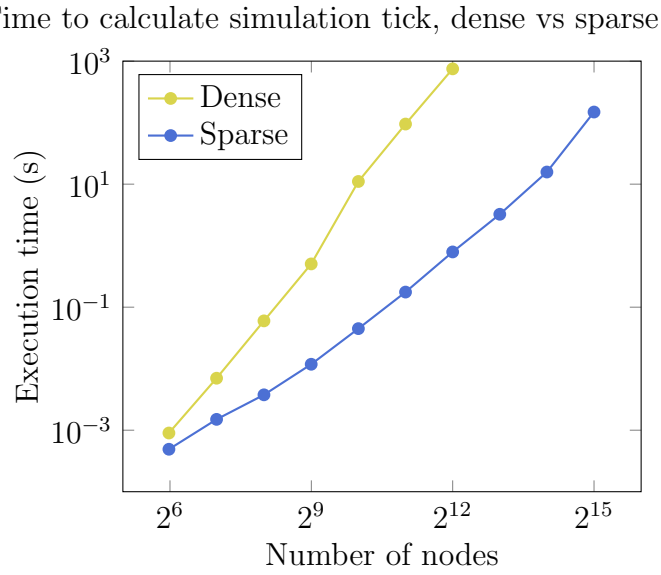

Figure 1: Time to compute a single simulation tick, with dense versus sparse matrices. Models were simulated for 10 ticks in total, with the results above taken as the average of the final 5, to reduce the impact of operating system caching on performance.

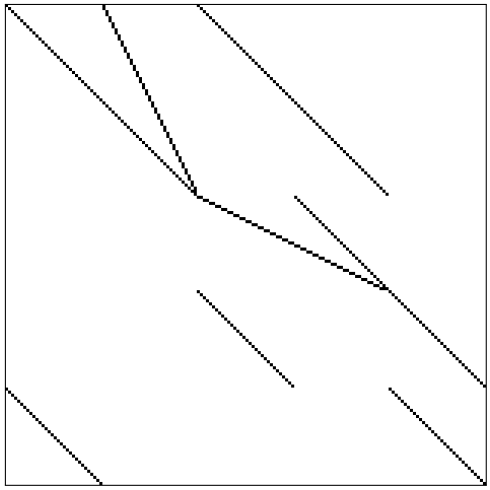

(a) The sparsity pattern of Jacobeans as implemented

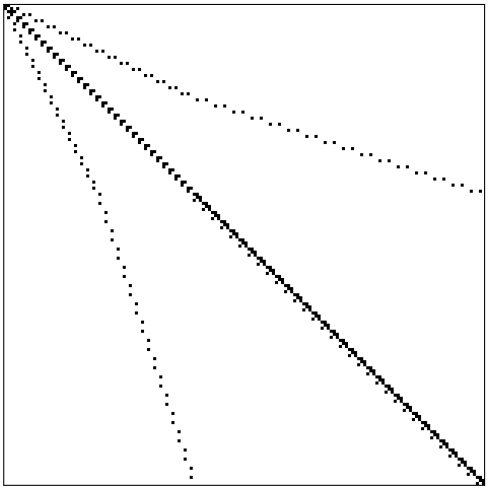

(b) A possible "cleaner" sparsity pattern, arranging variables for each node at consecutive indexes.

Figure 2: Comparison of the implemented sparsity pattern with one possible alternative (of many). 2b is not *necessarily* more efficient; it demonstrates that other options were available, as an area of possible improvement.

- Pleural pressure wave characteristics (initial value, mean, amplitude, and period)

The specification of "healthy" and "degraded" allows us to define and transition between two states of the lungs, simulating the onset and treatment of the affects from many respiratory illnesses. The speed of onset or recovery is controlled by the positioning of the keyframes, which are binary "healthy" or "degraded" states. These states do not directly affect the simulation state, i.e. the flow, pressure, and acinar volume within each branch. This does mean that, for example, the pressure in constricting airways does not increase directly as a result of that constriction, but we have considered the volume inside the branches themselves largely negligible. The most important factor is that the volume within each acinar region is conserved, which *is* guaranteed, even across changing compliance.

It is also worth clarifying the meaning of *relative compliance* in the list above. In order to ensure that the total volume of the lungs remains consistent with human anatomy, the compliance of each acinar region is linearly scaled so that the total volume from all acinar regions filled at atmospheric pressure is 2.0 liters.

Todo: **This should probably not be 2 liters; looking at the actual data, the starting volume of the lung doesn't really correspond to FRC *or* FRC + tidal volume, so it should be closer. There's also the issue that the tidal volume that the simulation reports is *much*, much less than what it should be – like... 40 milliliters kind of small.**

This *probably* has something to do with the compliances being much smaller than what Foy's paper had, but I'm still really not sure why that was happening.

A comparison and analysis of transition interpolation functions is given in section 4, alongside their definitions.

The details of the configuration format itself are outside the scope of this paper, but the configurable values are described here to provide context for the parameters that were varied in the experiments we report.

4 Results

4.1 Observed numerical stability

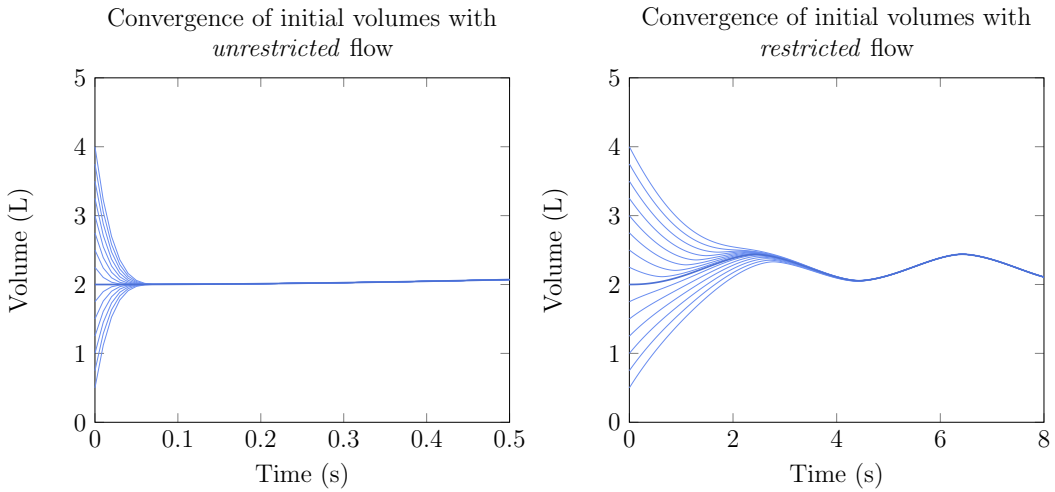

Figure 3: Simulated volume at the start of a breathing cycle, with varied initial volumes. Both experiments with a symmetric model with a depth of 6 (i.e., 63 total branches). Graphs display the distinction between unrestricted (left) vs 80% constricted (right). **Note:** displayed timespan differs between the left and right graphs.

To be confident in the results of other experiments, it is first crucial to determine that the simulation remains stable after running for extended periods of time. To do this, we simulated a simpler model (fully symmetric, no constriction, depth of 6) for 1000 seconds – which required 100,000 simulation ticks.

It is at this point that we'd ideally reference some figure to show that the system is stable in this configuration, but the series of volumes at each timestamp – starting at 0, 100, and 1000 seconds – were all the same, up to nine significant figures. In other words, total volume of air in the lungs over the course of each "breath" did not change over the course of an atypically lengthy experiment.

We also considered that the initial volume used in experimentation is not guaranteed to be accurate to the "typical" volume at that point in the breathing cycle – a fact that becomes visible with higher degrees of airway constriction (discussed in subsection 4.2). Therefore, we also experimented with significantly changed initial volumes, as shown above in Figure 3. The system quickly recovers from pertubations when airflow is unrestricted, but is slower to return to the typical volume when resistance prevents the correction from being made more quickly.

4.2 Flow characteristics under stable constriction

The first set of experiments investigated the behavior of sustained, normal breathing under minimal to severe constriction. Here, we used whole-lung constriction – limiting the radius of all airways by a given fraction. Figure 4 displays the recorded airflow at the larynx for normal breathing under a few different levels of constriction.

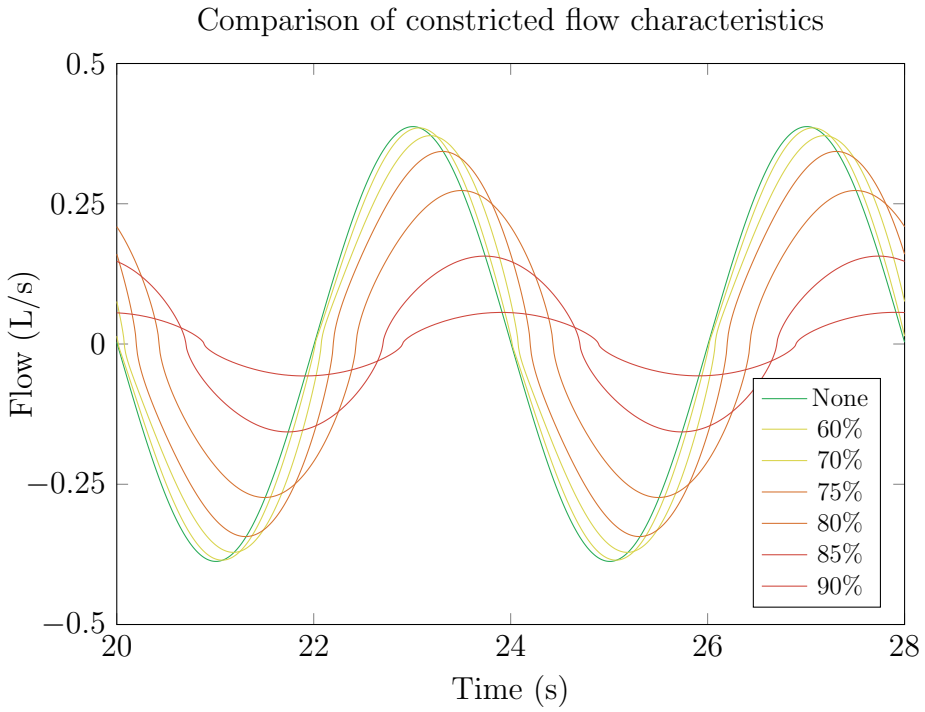

Figure 4: Stable flow during two breathing cycles with varied levels of whole-lung airway constriction. Measurements were only recorded after 20 seconds to ensure the effects of any starting conditions had been minimized, shown necessary at severe constriction by Figure 3.

The function determining pleural pressure was kept constant. Consistent with prior studies, the effects of constriction on airflow only become noticeable after significant constriction – in this case, 60-70%.

Todo: **need to directly name the prior studies, whatever I can find**

As constriction increases, there are three visible effects: the maximum flow starts to decrease, the time at which the maximum flow occurs starts to shift later, and the shape of the flow curve also changes – becoming flatter at its peaks and steeper around the transitions between positive and negative flow.

Figure 5 quantifies these effects. Maximum flow remains relatively constant until around 60-70% constriction, after which it steadily curves towards zero. However, before even the *amount* of flow changes, effects are readily visible in other characteristics of the curve – particularly the maximum acceleration: At only 50% constriction, the maximum acceleration has already increased by 27% (0.62 to 0.79 L/s^2) whereas the maximum flow has only decreased by 0.2% (0.3875 to 0.3868 L/s).

Some uneveness is present in the graph of maximum aceleration; this is likely in large part due to the method of measurement. Because acceleration was calculated only with the change in flow from one simulation tick to another, differences in the timing of this maximal acceleration have likely presented here as local differences in spite of the global trend.

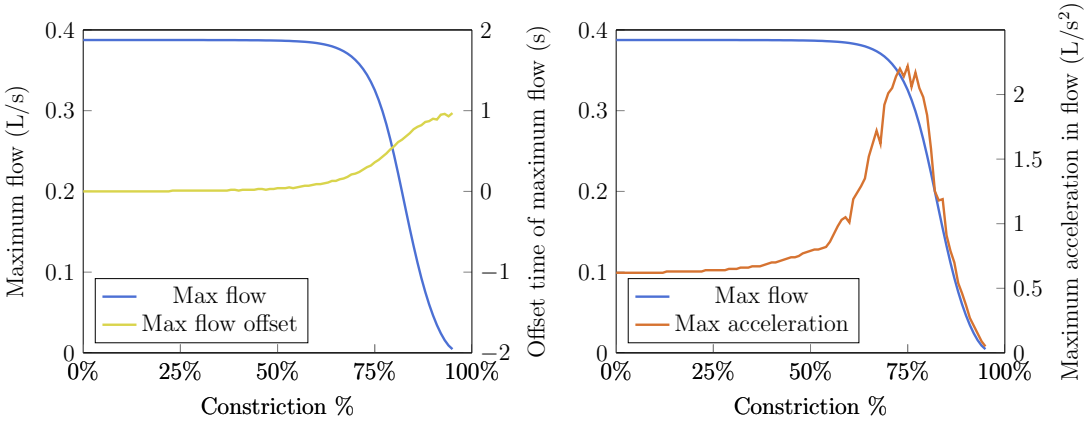

(a) Maximum flow and time it occurs relative to no constriction

(b) Maximum flow and maximum acceleration in flow

Figure 5: Quantified changes in airflow as constriction increases, up to 95%. Peak airflow is displayed as a baseline for both the time maximum flow occurs (left) and the maximum acceleration in flow between simulation ticks (right).

4.3 Comparison of interpolation functions

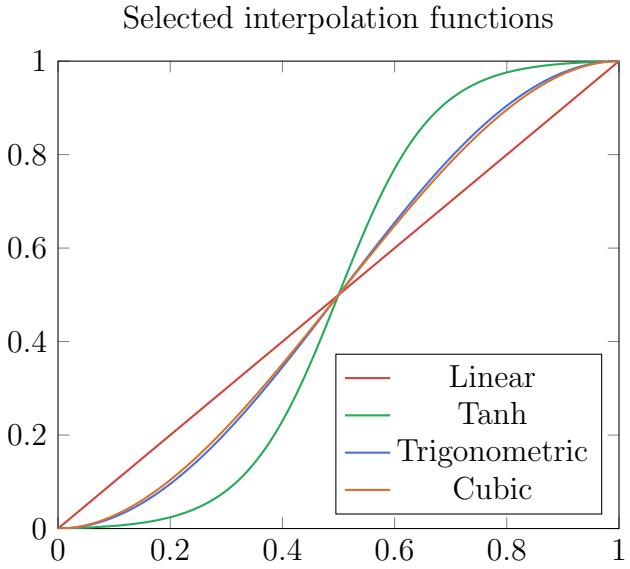

Figure 6: Comparison of the four selected interpolation functions

Later experiments explore the effects of rapid changes in airway constriction. To move between these "constricted" and "unconstricted" states, we have four different interpolation functions:

- *Linear*: $f(x) = x$
- *Tanh*: $f(x) = \frac{1}{2}\frac{\tanh(6x-3)}{\tanh(3)} + \frac{1}{2}$
- *Trigonometric*: $f(x) = \frac{1}{2}(1 - \cos(\pi x))$

- *Cubic*: $f(x) = 3x^2 - 2x^3$

A visual comparison of these functions is provided in Figure 6.

These functions were selected for their relative simplicity and variety of curvature.

Todo: **Explaining exactly why the curvature is necessary is escaping me right now. It's basically that the flow behaves extra weirdly without curvy interpolation, but that's not very scientific.**

There's an alternate angle, which is that curvy interpolation intentionally allows the significant changes at high constriction to happen more slowly (e.g. going 10% to 15% is much slower than 15% to 20%). This is "good" because flow characteristics change rapidly as you change constriction *from* high constrictions, so moving slowly ensures that the flow is less erratic.

On the other hand, maybe this is biasing the results and *actually* the erratic flow is more realistic. Would be good to discuss.

Todo: **The other piece of writing in this section is going to be a comparison of the flow characteristics when when switching on various interpolation methods.**

We eventually choose *Tanh*, basically because it looks the best (subject to change!). See above notes.

Finally, it is worth noting that the correction factor of tanh(3) in the denominator of the *Tanh* interpolation function is nearly equal to 1, but still necessary. The value of tanh(3) is only 0.995, but experiments without that correction factor showed clearly visible instantaneous changes in flow from that small change. While these changes were most likely harmless, we still elected to remove them.

5 Recovery

Todo: **fill this in**

6 Asymmetric constriction

Todo: **fill this in**

7 Discussion

7.1 Summary of key results

Todo: **all of this**

7.2 Limitations and further work

Todo: **all of this**

References

[1] The global impact of respiratory disease – second edition.

[2] B. Foy. Computational models of pulmonary function tests, 2018.